Creep of un-doped and Cr-doped WC-Co at high temperature and high load

International Journal of Refractory Metals and Hard Materials 117 (2023) 106417

Contents lists available at ScienceDirect

International Journal of Refractory Metals and Hard Materials

journal homepage: www.elsevier.com/locate/IJRMHM

Creep of un-doped and Cr-doped WC-Co at high temperature and high load

M.A. Yousfi [a,1], A. Nordgren [b], S. Norgren [b,c], J. Weidow [a,*], H.-O. Andrén [a], L.K.L. Falk [a]

[a] Department of Physics, Chalmers University of Technology, SE-412 96 Göteborg, Sweden
[b] Sandvik AB, R&D Materials and Processes, SE-126 80 Stockholm, Sweden
[c] Department of Mechanical Engineering, Lund University, SE-223 62 Lund, Sweden

ARTICLE INFO

Keywords:
Cemented carbide
High temperature deformation
Grain growth
Phase boundary segregation
Binder phase lamella
Grain boundary sliding

ABSTRACT

Un-doped and Cr-doped WC-10 vol% Co cemented carbides with a WC grain size of 1.4 μm have been investigated before and after hot compressive creep tests under an applied load of 900 MPa at 1000 °C and 300 MPa at 1100 °C. The Cr-doped material showed a much higher creep resistance at 1000 °C and a somewhat higher creep resistance at 1100 °C than the un-doped material. Quantitative microscopy showed that WC grain growth occurred in the plane perpendicular to the load axis during creep deformation and that the growth process was slower in the Cr-doped material. In addition, binder phase redistributed and a number of WC grain boundaries were infiltrated with binder phase. This suggests that accommodated WC grain boundary sliding occurred during creep deformation. The formation of intergranular cavities implies that also unaccommodated grain boundary sliding occurred, especially at 1000 °C. It is suggested that WC grain growth perpendicular to the load axis is rate limiting in the creep deformation process, and that Cr segregation to WC/binder phase boundaries hinders grain growth. The weak effect of Cr on creep resistance at 1100 °C at 300 MPa is explained by Cr giving a larger volume fraction of binder phase and therefore a larger number of infiltrated grain boundaries, facilitating grain growth.

1. Introduction

The use of WC-Co cemented carbides as cutting tool materials often involves high working loads at high temperatures. Temperatures as high as 1000 °C, locally even up to 1100 °C, may sometimes be reached during turning operations [1] and the tool is subjected to a high load during a certain period of time. Under these conditions, the tool lifetime may be affected not only by various wear mechanisms but also by limitations in the mechanical properties of the cemented carbide. The high constant load in a turning operation may, for example, cause creep deformation of the tool.

There is a considerable interest in improving the high temperature properties of these composite materials by modifying their composition and microstructure. The deformation mechanisms, as well as the evolution of microstructure at elevated temperatures, are not well understood, however. High temperature creep testing is a good way to simulate the conditions under service in order to study the behaviour of the material in a controlled way.

The creep behaviour of cemented carbides has previously been investigated in three- and four-point bending tests [2–7] and by tensile [8–12] and compressive [3,10,12–16] creep testing. The compressive creep tests were carried out at temperatures ranging from 700 °C to 1350 °C.

Microstructure investigation after tensile creep testing at 900 °C found evidence of WC grain boundary decohesion and some evidence of grain boundary sliding [9]. Creep tests carried out in three-point bending have, with the aid of photolithography, shown that grain boundary sliding might be a mechanism of deformation at temperatures around 900 °C [5]. These creep tests also resulted in a decohesion of WC grain boundaries [5]. The formation of Co-rich films in WC grain boundaries has clearly been observed also after compressive creep testing at 1000 and 1100 °C [15] and in the microstructure of used cemented carbide cutting tools [1,7,17]. The formation of these Co-rich grain boundary films has been suggested to indicate deformation by accommodated grain boundary sliding [7,15,17,18].

Using mechanical spectroscopy Buss found that grain boundary sliding becomes the dominating deformation mechanism above 1100 K (823 °C) in WC-Co [18]. She suggested that there are two stress regimes of grain boundary sliding in WC-Co cemented carbide materials: limited grain boundary sliding at low stress, related to the inherent segregation

* Corresponding author.
E-mail addresses: amine.yousfi@ri.se (M.A. Yousfi), jonathan.weidow@chalmers.se (J. Weidow).
[1] Present address: Research Institutes of Sweden, Argongatan 30, SE-431 53 Mölndal, Sweden.

https://doi.org/10.1016/j.ijrmhm.2023.106417
Received 29 March 2023; Received in revised form 27 August 2023; Accepted 4 September 2023
Available online 29 September 2023

of Co to the WC grain boundaries, and extensive grain boundary sliding at high stress, facilitated by infiltration of Co into the WC grain boundaries [18]. Molecular dynamics simulations have demonstrated that at temperatures up to 1200 °C, a WC grain boundary infiltrated by six or more atomic layers of Co requires a one order of magnitude smaller shear stress to slide, compared to boundaries without Co infiltration (containing the usual half monolayer segregation of Co) [19].

Plastic deformation of the WC skeleton and the Co-rich binder phase may also occur during creep testing. Creep deformation of the WC grains resulted in an increased intragranular dislocation density [3,5,9,15]. A redistribution of the Co-rich binder phase has also been observed during creep testing [15]. The comparatively large (> 50 μm) binder phase grain size [20] was reduced, and the finger-like grain morphology was lost [15]. Formation of intergranular cavities during creep testing has also been reported by many authors [1,2,8,11,15].

In addition to the phenomena discussed above, WC grain growth has been observed during creep testing at 1000, 1100 and 1200 °C [14,15,21]. The work by Yousfi et al. showed that this growth takes place preferentially perpendicular to the compressive load axis during creep deformation. It was suggested that intragranular dislocations merging on the WC grain surfaces may, provided that they have a screw component, constitute a nucleation site for WC grain growth [15].

During cemented carbide production it is common to make different additions to the powder mixture to prevent WC grain growth during sintering. For example, chromium is a well known WC grain growth inhibitor [22,23]. Today, additions of up to 0.4 wt% Cr (0.5 wt% Cr_3C_2) are commonly made [24]. However, there is little knowledge on what effects larger additions of chromium have at high temperature applications.

The present investigation is concerned with compressive creep testing of an un-doped and a Cr-doped WC-Co cemented carbide material at 1000 and 1100 °C using high loads, 900 and 300 MPa, respectively. Temperatures and loads were chosen to be representative for the conditions on the rake face of a tool during a metal turning operation. Locally, temperatures around 1000 °C and loads up to 2000 MPa are then expected [25–28]. The work was carried out in order to isolate the effect of Cr additions. The two materials were designed to have the same WC grain size and the same volume fraction of the Co-rich binder phase. The microstructures before and after creep testing were characterized in the scanning electron microscope (SEM) in order to create an understanding of the deformation process and to identify relevant deformation mechanisms.

2. Experimental procedures

2.1. Material production

The creep behaviour of two experimental materials was investigated: WC with 6.00 wt% Co and WC with 6.00 wt% Co and 0.60 wt% Cr, see Table 1. These compositions are expected to result in ~10 vol% of Co-rich binder phase in the sintered materials.

The two materials were designed so that they would end up with the same WC grain size after sintering. Since Cr is a well-known WC grain growth inhibitor, and because of the Cr-doping of one of the materials in this work, two different WC starting powders with different average WC particle sizes were used. The WC powder supplier was in both cases Wolfram Bergbau AG. The WC powders used for the un-doped and Cr-doped materials had FSSS values of 5.6 and 6.25 μm, respectively. The Co powder was from Umicore and had an average particle size of 0.8 μm. The Cr_3C_2 added to the doped material came from Treibacher and had a FSSS size of 1.6 μm.

Starting powder mixtures containing WC + Co or WC + Co + Cr_3C_2, and an addition of 2 wt% polyethylene glycol as pressing agent, were ball milled in ethanol–10% H_2O in a stainless steel mill for 11.5 h.

The slurries were spray dried, and the granules were isostatically pressed into cylindrical green bodies. The green bodies were machined into the shape of a test bar, and then gas pressure sintered at 1410 °C under 55 bar Ar pressure with a holding time of one hour. The final dimensions of the test bars after shrinkage during sintering and final grinding of the grip were 42 mm in length, a grip diameter of 12 mm, a smallest diameter of the gauge length of 6.3 mm, and a gauge length of 12 mm, see Fig. 1. The magnetic saturation measurements ($(Co)_m/Co$) showed that the two materials had nearly the same carbon potential, see Table 1. This means that the Co-rich binder phases in the two materials would contain similar amounts of dissolved W and C.

2.2. Creep tests

Compressive creep tests were carried out at 1000 °C under a stress of 900 MPa and at 1100 °C under a stress of 300 MPa, see Table 2.

The relationship between stress (σ) and strain rate ($\dot{\varepsilon}$) in the intermediate steady state creep regime may be expressed by

$$\sigma = \left(A' \dot{\varepsilon} exp\frac{E}{kT}\right)^m$$

where A' is a constant, m the strain rate sensitivity, T the creep temperature, E the activation energy, and k is Boltzmann's constant [29]. Provided that the same creep mechanisms are active at 1000 and 1100 °C, the stress has, hence, to be reduced at the higher temperature in order to deform at the same strain rate. Previous work has identified an activation energy of $E = 6$ eV and a strain rate sensitivity of $m = 0.28$ at test temperatures above 1100 K (827 °C) [18]. Based on these data, the stress was reduced to 300 MPa in the creep experiments carried out at 1100 °C in order to deform at the same strain rate and stay in the intermediate steady state creep regime.

During the compressive creep test, the sample was placed between cylindrical ceramic discs (SiC whisker reinforced alumina, Coromant insert grade GC670) with diameter of 15 mm and a thickness of 8 mm, to prevent the cemented carbide from cracking and reacting with the holder and to work as a thermal isolator to reduce temperature gradients in the sample. An induction coil was used for heating. Knowing that induction heating might give temperature gradients in the material, test runs were done with three spot welded thermocouples, (Pt-Pt/Rd), on a sister sample, to position the coil until the temperature gradients where <10° between the top and bottom point of measurement, see Fig. 2).

Table 1
Composition and data of the materials investigated in this work.

Material	Composition[a]			Binder phase [vol%]	Materials data		
	Co [wt %]	Cr [wt %]	C [wt %]		H_c [kA/m]	$(Co)_m/Co$	HV3
WC-Co	6.00	–	5.70	10	10.42	0.90	1393 ± 25
WC-Cr-Co	6.00	0.60	5.73	10	10.15	0.93	1418 ± 25

[a] Balance W.

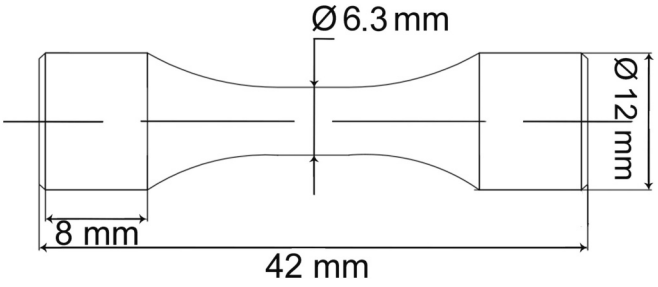

Fig. 1. The test bar geometry.

Table 2
Creep data of the investigated materials.

Material	Temperature [°C]	Stress [MPa]	Strain [%]	Time [s]
	1000	900	9.9	923
Un-doped	1000	900	19.9[a]	1386
	1100	300	8.7	1800
	1000	900	9.9	2405
Cr-doped	1000	900	17.1[b]	3345
	1100	300	7.5	1800

[a] Cracked WC grains.
[b] Test bar fractured.

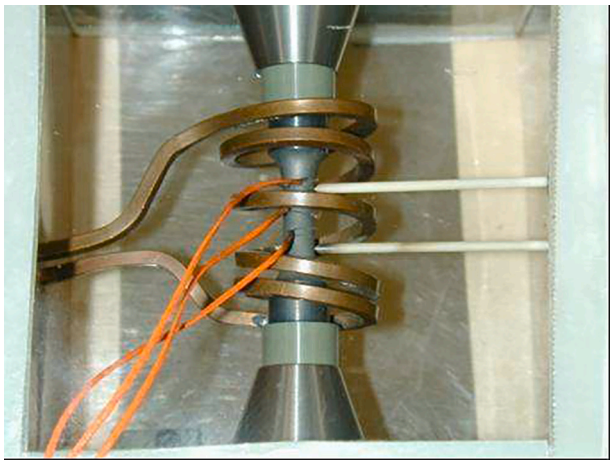

Fig. 2. Position of sample, extensometers, thermocouples and ceramic discs (green). (For interpretation of the references to colour in this figure legend, the reader is referred to the web version of this article.)

During the creep test only one thermocouple in the middle position was used. The deformation was measured as the reduction in length, ($\varepsilon = \Delta L/L$), using an extensometer, over a length of 12 mm via two alumina rods, (Ø2 mm, length 100 mm). The 10% range of the extensometer made it necessary to conduct the 20% creep test in two runs. To prevent oxidation a box was constructed around the setup. The box was filled with argon and then a low flow of argon gas was applied. The intention was to interrupt the creep tests when a lower (around 10%) and a higher (around 20%) strain had been obtained at 1000 °C, and when around 10% strain had been obtained at 1100 °C. The temperature dropped very quickly when the heating was turned off; cooling of the test bars from 1100 down to 800 °C took only 19 s. The 10% strain was chosen to emulate real cutting conditions and the 20% strain as an exaggeration to possibly easier draw conclusions from the experiments.

The recorded creep curves all consisted of a first part with decreasing creep rate (primary creep) and a second part with constant creep rate (secondary creep). In some cases, also a third part with increasing creep rate was present (tertiary creep). The strain at which onset of secondary creep occurred was determined by modelling the creep curve as a sum of an exponential and a linear curve. The onset was then taken as the strain at which the strain from secondary creep exceeded that of primary creep.

2.3. Microstructural characterization

Metallographic specimen preparation of sections cut from the as-sintered test bars of the two materials was done by mechanical polishing using diamond spray, down to 1 μm particle size, followed by chemical etching in Murakami's reagent for two minutes at room temperature [30]. The prepared sections were investigated by optical microscopy in order to identify any abnormal grain growth during sintering of these materials.

Specimens for scanning electron microscopy (SEM) were cut from the gauge length of the test bars using a high-speed diamond saw. Two sections in the as-sintered and crept test bars were investigated. One slice of the gauge length was cut perpendicular to the load axis, and another slice parallel to the axis, see Fig. 3. The slices had a thickness of 250 μm and were taken from the centre of the gauge length.

The surfaces of the slices were mechanically polished with diamond spray, down to 1 μm particle size finish. For a better surface quality, and a residual stress-free surface, the polished surfaces were ion etched in a Gatan precision ion polishing system (PIPS). Sputtering was carried out for two hours with a 4 keV Ar^+ ion beam at an incident angle of 2°.

Backscattered electron imaging was done at 5 kV in a Leo Ultra 55 FEG-SEM equipped with an Oxford INCA system for X-ray energy dispersive spectrometry (XEDS). A magnification of 17,000× was set on the SEM, and three areas of approximately 50 μm by 45 μm were investigated on each section: at the centre, at half radius distance from the centre, and just below the surface of the gauge length (rim), see Fig. 3. The image resolution was set to 1024 × 768 pixels, giving a pixel size of 16 by 16 nm^2.

The average WC grain size was determined by the linear intercept method [31]. Intercept lengths were determined in two perpendicular directions on the cross section taken perpendicular to the load axis, and in directions perpendicular and parallel to the load axis on the sections cut parallel to the axis. A 95% confidence interval (CI) was determined for the average grain size from:

$$95\%\mathrm{CI} = t.\ s.\ n^{-1/2}$$

where s is the standard deviation of the measured intercept lengths, n is the number of measured intercepts, and the factor t is a multiplier related to the number of fields that were analysed. In this study t was set to 2.571 (six fields) or 2.776 (five fields) [32].

The backscattered electron images taken for the linear intercept measurements were converted to binary images with the purpose to estimate the intergranular volume fraction of the two materials before and after creep deformation. After adjustment of the contrast threshold level in the electron micrographs, the Co-rich binder phase appears with black contrast and the WC grains with white contrast. The image area fraction of WC grain sections is then given by the average pixel value. The intergranular area fraction is given by 1 minus this value. The WC grains and the binder phase pools are randomly distributed and oriented in these microstructures. It may, hence, be assumed that the determined intergranular area fraction is a good estimate of the intergranular volume fraction.

The backscattered images taken for the linear intercept measurements were also used for the determination of the number density of WC grain boundaries containing a film of the Co-rich binder phase (i. e. the number of film containing grain boundaries per unit section area). From the imaging conditions used it may be expected that grain boundary film thicknesses down to around 50 nm would be detected.

To produce specimens for transmission electron microscopy (TEM) 250 μm thick slices were cut from the test pieces. The slices were thinned to a thickness of 150 μm on a 15 μm diamond grinding disc and then polished on both faces using a diamond spray of 1 μm particle size. Discs with a diameter of 3 mm were cut from the thin slices using an ultrasonic disc cutter, and subsequently dimple ground on both sides down to a centre thickness of 50 μm. Final thinning to electron transparency was carried out by ion milling with 4 keV argon ion beams incident on both sides of the specimen at an angle of 10°. The TEM specimens were investigated in a FEI Tecnai T20 microscope.

2.4. Thermodynamic modelling

To estimate how the volume fraction of binder phase depends on temperature, equilibrium calculations were made using Thermo-Calc version 2022a. The thermodynamic database used for the W-C-Co-Cr

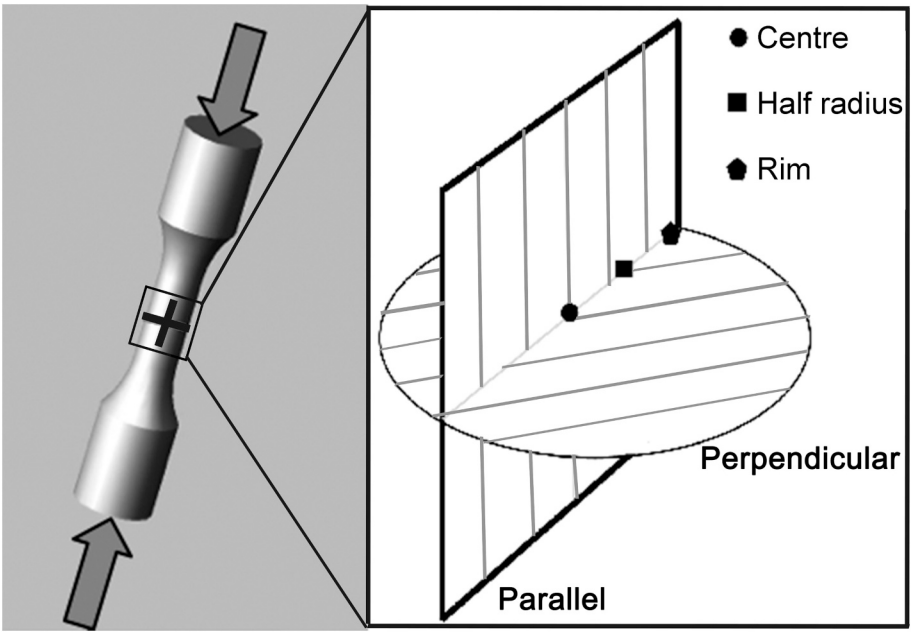

Fig. 3. The two cross-sections, parallel and perpendicular to the load axis, taken from the test bars. The three areas (centre, half radius distance from the centre and rim) investigated on the sections are indicated.

system was TCFE7.

3. Results

3.1. Microstructure of as-sintered materials

Pure WC-Co cemented carbides may, in some cases, exhibit abnormal WC grain growth during sintering [33]. This is one reason why grain growth inhibitors like Cr or V are usually added to WC-Co materials [22,23]. An inspection in the optical microscope, however, did not reveal any abnormal grain growth during sintering of the two WC-Co cemented carbide materials studied in this investigation, see Fig. 4. The general microstructure of the two materials is shown at a higher magnification in Fig. 5. The un-doped material showed the typical two-phase structure of a WC-Co cemented carbide, i.e. WC grains embedded in a Co-rich binder phase. The Cr-doped material showed, in addition, the presence of a limited number of smaller grains of chromium carbide (Fig. 5b). These grains had a size of around 0.5 μm, and they had mostly grown on WC grain surfaces. The WC grains in the two as-sintered materials appeared to form a continuous skeleton penetrated by the Co-rich binder phase. The binder appeared, mostly, in pockets at WC multigrain junctions in the SEM images (Fig. 5). Most of the WC/WC and WC/binder phase interfaces in the as-sintered materials had a straight appearance, and the microstructures did not show any porosity in the SEM images. TEM imaging revealed that there were few and short dislocations in the WC grains but more defects in the binder phase (Fig. 6).

The mean WC linear intercept lengths perpendicular and parallel to the axis of the as-sintered un-doped test bars were (1.39 ± 0.06) μm and (1.38 ± 0.08) μm, respectively. The Cr-doped as-sintered test bars had linear intercept lengths of (1.41 ± 0.06) μm perpendicular to, and (1.39 ± 0.09) μm parallel to the axis, see Table 3. These values result in an average WC grain size of (1.39 ± 0.07) μm in the un-doped material and (1.40 ± 0.08) μm in the Cr-doped material.

The experimentally determined intergranular volume fractions in the un-doped and Cr-doped materials were (10.1 ± 0.3) % and (9.9 ± 0.3) %, respectively, see Table 4. These numbers are virtually the same as the volume fraction of Co-rich binder phase (10%) expected from the starting powder compositions.

Only a limited number of WC grain boundaries in the as-sintered materials contained a film of the Co-rich binder phase (binder phase lamella). The number density of film containing grain boundaries, as determined from the SEM images, were (5.5 ± 1.2) × 10^{-3} μm^{-2} in the

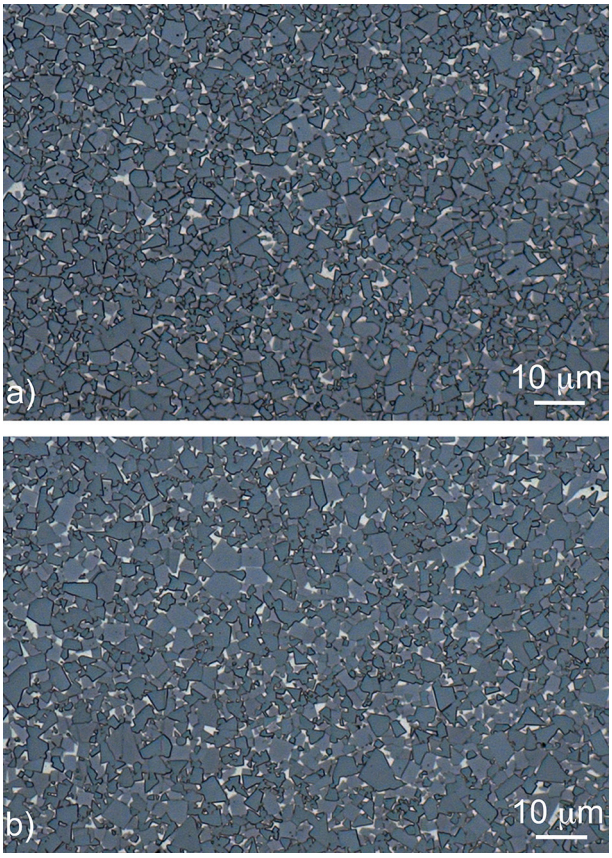

Fig. 4. Optical micrographs of etched surfaces from the as-sintered un-doped (a) and Cr-doped (b) materials. The Co-rich binder phase appears with bright contrast.

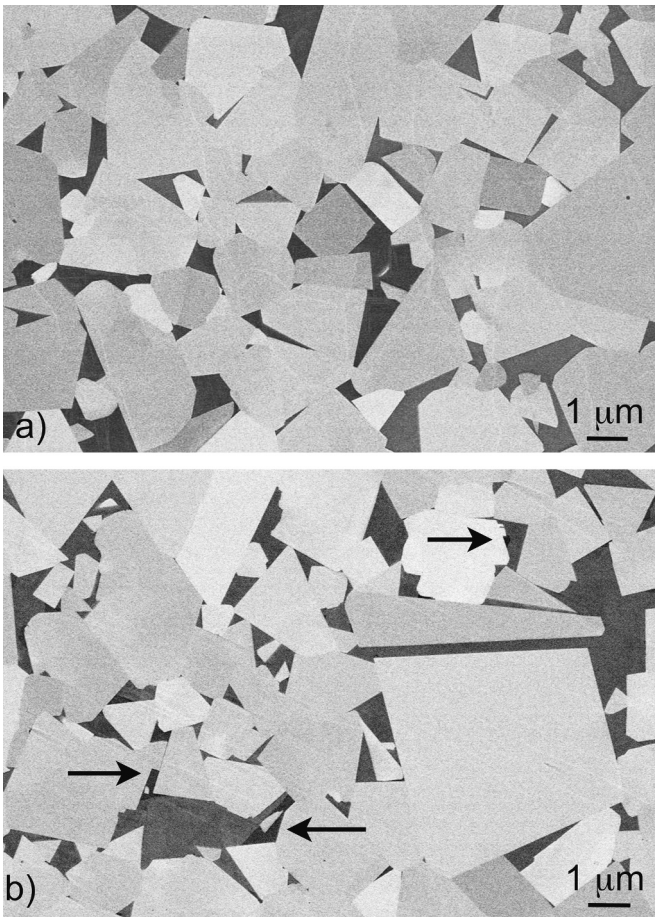

Fig. 5. The general microstructures of the as-sintered un-doped (a) and Cr-doped (b) materials (SEM micrographs). Cr carbide particles in the Cr-doped material are arrowed in (b). The WC gains appear with bright contrast, the binder phase with dark, and the Cr carbides with black contrast.

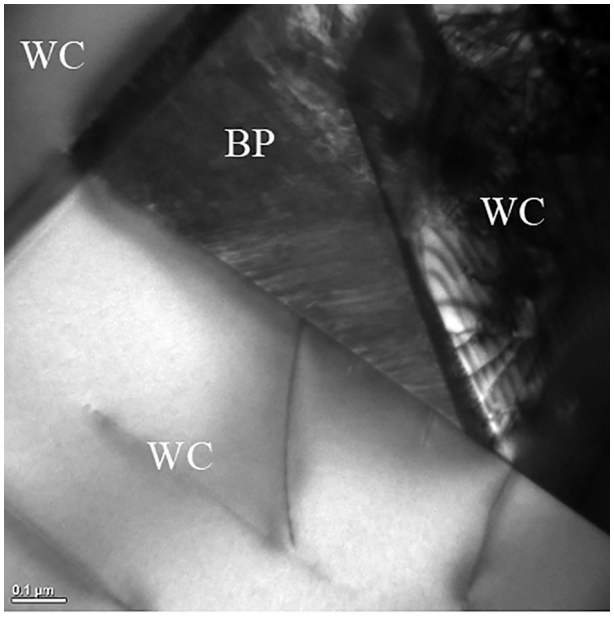

Fig. 6. TEM micrograph of the un-doped material. Few dislocations only are found in the WC grains, whereas the binder phase (BP) contains more defects.

un-doped material and (6.9 ± 0.6) × 10^{-3} μm^{-2} in the Cr-doped material, see Table 5.

Table 3
Mean linear intercept length of WC grain sections.

Material	Mean linear intercept length (μm)	
	Un-doped	Cr-doped
As-sintered		
Perpendicular to load axis	1.39 ± 0.06	1.41 ± 0.06
Parallel to load axis	1.38 ± 0.08	1.39 ± 0.09
Crept at 1000 °C	9.9% strain, 923 s	9.9% strain, 2405 s
Perpendicular to load axis	1.58 ± 0.06	1.59 ± 0.06
Parallel to load axis	1.39 ± 0.09	1.38 ± 0.08
Crept at 1100 °C	8.7% strain, 1800 s	7.5% strain, 1800 s
Perpendicular to load axis	1.51 ± 0.06	1.50 ± 0.06
Parallel to load axis	1.38 ± 0.08	1.38 ± 0.08

Table 4
Intergranular volume fraction.

Material	Intergranular volume fraction (%)
Un-doped	
As-sintered	10.1 ± 0.3
1000 °C, 9.9% strain, 900 MPa	12.9 ± 0.3
1100 °C, 8.7% strain, 300 MPa	11.2 ± 0.3
Cr-doped	
As-sintered	9.9 ± 0.3
1000 °C, 9.9% strain, 900 MPa	13.1 ± 0.3
1100 °C, 7.5% strain, 300 MPa	11.6 ± 0.3

3.2. Creep tests

The strain vs. time curves recorded during creep testing at 1000 °C are presented in Fig. 7. The two creep tests of the un-doped material were interrupted after 923 s at a strain of 9.9%, and after 1386 s at a strain of 19.9%, see Fig. 7 and Table 2. The Cr-doped material showed a significantly higher creep resistance. The creep tests of this material were interrupted after 2405 s at 9.9% strain, and, due to fracture, after 3345 s at a strain of 17.1%, see Fig. 7 and Table 2. As shown in Fig. 7, the two creep tests carried out to 9.9% strain were interrupted in the steady state regime. The tests carried out to higher strains (19.9 and 17.1%) were both interrupted in the tertiary stage of accelerating creep, see Fig. 7b.

The transition from primary to steady state creep at 1000 °C was at around 4.5% strain after around 255 s for the un-doped material (Fig. 7a). The Cr-doped material showed a longer stage of primary creep, and the transition to steady state creep occurred at around 6.1% strain after around 1010 s (Fig. 7a). The steady state creep rate of the un-doped material at 1000 °C was determined to 8.6 × 10^{-3} s^{-1} from the creep curves. The Cr-doped material had a significantly lower steady state creep rate, 2.8 × 10^{-3} s^{-1}, at this temperature.

Fig. 8 shows the strain-time curves recorded during creep testing at 1100 °C. The creep test of the un-doped material was, in this case, interrupted after 1800 s at a strain of 8.71%, see Fig. 8 and Table 2. The Cr-doped material showed a slightly higher creep resistance, and reached a strain of 7.50% after 1800 s, see Fig. 8 and Table 2. The creep deformation of the un-doped and Cr-doped test bars at 1100 °C was, hence, interrupted after 1800 s in both cases. At this stage, the deformation process was in the steady state creep regime, see Fig. 8.

The transition from primary to steady state creep at 1100 °C occurred at approximately the same strains as in the tests carried out at 1000 °C. The time spent in primary creep was, however, considerably longer (Fig. 7). The transition from primary to steady state creep occurred after 798 s for the un-doped material and after 1166 s for the Cr-doped material. The steady state creep rates at 1100 °C were determined to 4.3 × 10^{-3} and 2.9 × 10^{-3} s^{-1} for the un-doped and Cr-doped test bar, respectively.

Table 5
Number density of binder phase infiltrated WC grain boundaries.

Test bar section		Un-doped, number density [$\times 10^{-3}$ μm^{-2}]			Cr-doped, number density [$\times 10^{-3}$ μm^{-2}]		
		Centre	Rim	Average	Centre	Rim	Average
As-sintered	Parallel[a] Perpendicular[b]			5.5 ± 1.2			6.9 ± 0.6
Crept 1000 °C 9.9% strain	Parallel[a]	27.0	30.0	28.5 ± 1.5	31.6	30.7	31.2 ± 0.5
	Perpendicular[b]	31.0	43.1	37.1 ± 6.1	39.3	41.3	40.3 ± 1.0
Crept 1100 °C 1800 s	Parallel[a]	12.5	25.1	18.8 ± 6.3	24.7	31.3	28.0 ± 3.3
	Perpendicular[b]	12.1	28.9	20.5 ± 8.4	41.0	54.8	47.9 ± 6.9

[a] Section parallel to the load axis.
[b] Section perpendicular to the load axis.

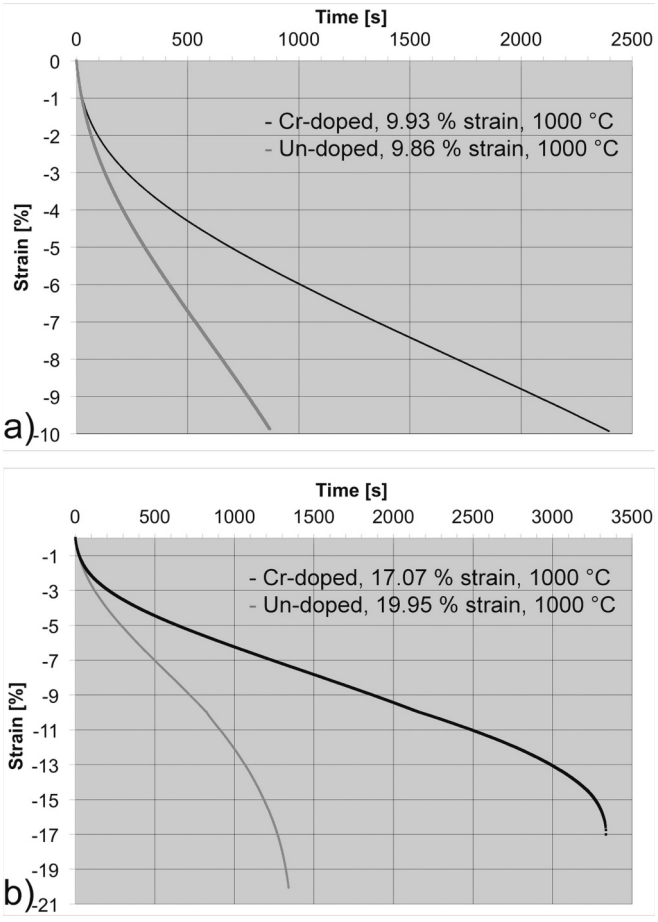

Fig. 7. Compressive creep curves registered during creep testing at 1000 °C. The un-doped material was deformed to 9.9% (a) and 19.9% (b) strain, and the Cr-doped material to 9.9% (a) and 17.1% (b) strain.

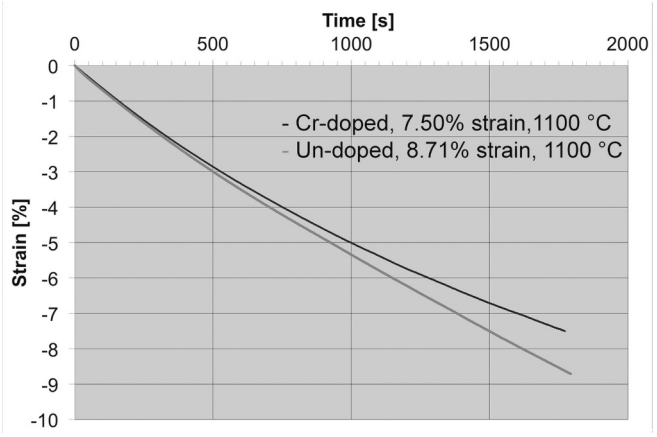

Fig. 8. Compressive creep curves registered during creep testing at 1100 °C. The un-doped material was deformed to 8.7% strain and the Cr-doped material to 7.5% strain.

3.3. Microstructure of creep tested materials

3.3.1. Creep tests at 1000 °C

The microstructures of the test bars crept at 1000 °C had a very different appearance compared to the as-sintered microstructures. The WC skeleton did not appear continuous any longer; many of the WC grain boundaries were penetrated by the Co-rich binder phase, see Figs. 9 and 10. In addition, intergranular cavities had formed during creep testing, see Figs. 9a and 10a. Many of the WC grain surfaces facing the Co-rich binder phase present between adjacent WC grains showed a saw-tooth like morphology, see Figs. 9b and 10b. The Cr carbides were present in the Cr-doped material also after creep testing at this temperature. TEM revealed that there were some dislocations in the WC grains that appeared longer than in the as-sintered material and perhaps also split into partial dislocations, as expected for gliding dislocations in WC [34] (Fig. 11a). There were also some dislocations in the binder phase.

The mean WC linear intercept length perpendicular to the axis of the test bar (i.e. the load axis) had increased after creep deformation to a strain of 9.9% at 1000 °C, see Table 3. This intercept length was determined to (1.58 ± 0.06) μm and (1.59 ± 0.06) μm for the un-doped and Cr-doped material, respectively, see Table 3. The intercept lengths determined parallel to the test bar axis were, on the other hand, virtually unchanged as compared to the as-sintered conditions. These values were (1.39 ± 0.09) μm for the un-doped material and (1.38 ± 0.08) μm for the Cr-doped material, see Table 3.

A large number of cavities were observed in the binder phase in the test bars crept to 9.9% strain at 1000 °C, see Figs. 9a and 10a. This was reflected in the pronounced increase in the intergranular volume fractions determined in these microstructures, see Table 4. The un-doped material had an average intergranular volume fraction of (12.9 ± 0.3) %, and the Cr-doped material had an average intergranular volume fraction of (13.1 ± 0.3) % (Table 4).

The number of WC grain boundaries containing a film of the Co-rich binder phase had clearly increased during creep testing at 1000 °C to a strain of 9.9%, see Figs. 9 and 10 and Table 5. In addition, the sections taken perpendicular to the load axis showed a clear difference between the centre of the crept test bar and the rim; the number density of binder phase containing WC grain boundaries was higher near the rim than in the centre of the test bar, see Table 5. A similar trend was also observed on the section taken parallel to the load axis from the un-doped test bar (Table 5). Furthermore, the sections taken perpendicular and parallel to

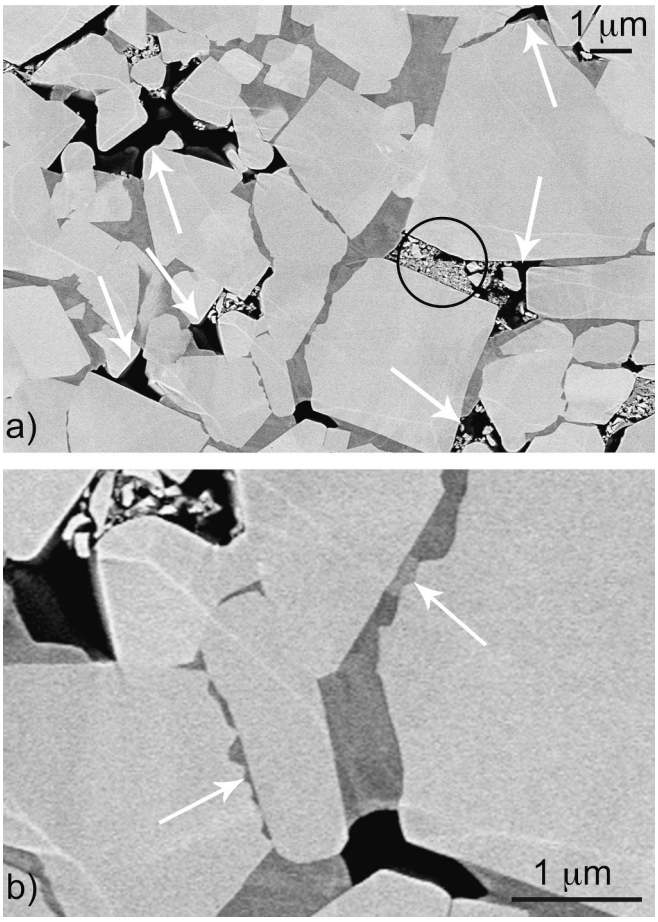

Fig. 9. (a) The general microstructure of the un-doped material crept at 1000 °C to 9.9% strain. WC grains appear with bright contrast, the binder phase with dark, and cavities (arrowed) with black contrast. There is debris from the specimen preparation (encircled example). (b) A higher magnification detail showing Co-rich films at WC grain boundaries where two of the WC grains have a saw-tooth like appearance (arrowed).

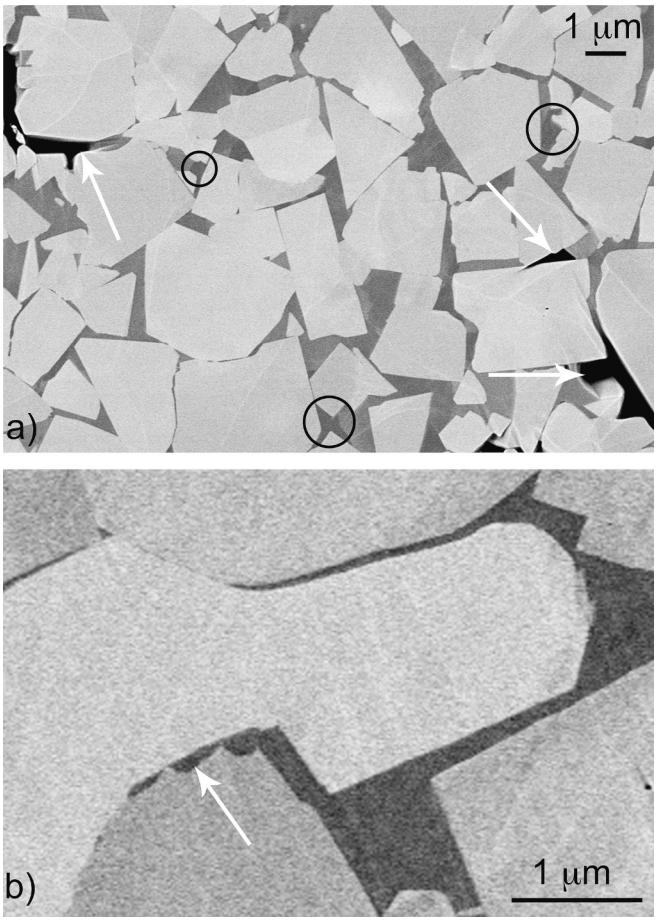

Fig. 10. (a) The general microstructure of the Cr-doped material crept at 1000 °C to 9.9% strain. WC grains appear with bright contrast, the binder phase with dark, chromium carbide with slightly darker (encircled examples) and cavities (arrowed) with black contrast. (b) A higher magnification detail showing Co-rich films at WC grain boundaries. One WC grain surface has a saw-tooth like appearance (arrowed).

the load axis of a crept test bar showed different number densities of film containing grain boundaries; a higher number density was observed in the section taken perpendicular to the load axis, see Table 5. The average number density of film containing grain boundaries in the crept un-doped test bar was determined to $(37.1 \pm 6.1) \times 10^{-3}$ μm^{-2} and $(28.5 \pm 1.5) \times 10^{-3}$ μm^{-2} for the perpendicular and parallel sections, respectively (Table 5). The crept Cr-doped test bar had an average number density of $(40.3 \pm 1.0) \times 10^{-3}$ μm^{-2} and $(31.2 \pm 0.5) \times 10^{-3}$ μm^{-2} on the perpendicular and parallel sections, respectively (Table 5). The Cr-doped material showed, hence, a higher number density of WC grain boundaries containing a film of the Co-rich binder phase than the un-doped material after creep testing to 9% strain at 1000 °C. The difference is particularly clear when comparing the sections taken perpendicular to the load axis, see Table 5.

The microstructure of the un-doped material crept to 19.9% strain at 1000 °C contained a large number of fractured WC grains, see Fig. 12a. A determination of an average WC grain size in this microstructure by the linear intercept technique would, hence, not give purposeful results. In addition, radial cracks extending from the surface of the gauge length were observed on the cross-section perpendicular to the load axis, see Fig. 12b. It should be noted that the un-doped test bar crept to 9.9% strain at this temperature did not show any crack formation.

The creep test of the Cr-doped material aimed at the deformation to the higher strain (around 20%) at 1000 °C resulted in fracture of the test bar at 17.1% strain. The fracture surface had an intergranular appearance below the surface of the gauge length, see Fig. 13a. This morphology changed when approaching the centre of the test bar, where a more smeared appearance of the fracture surface was observed, see Fig. 13b. Radial cracks extending inwards from the surface of the gauge length had, most likely, been initiated comparatively early in the deformation process under the applied compressive creep conditions. Shorter cracks at the surface of the gauge length of the Cr-doped test bar were observed on the cross-section perpendicular to the load axis after creep deformation to 9.9% strain at 1000 °C, see Fig. 14.

3.3.2. *Creep tests at 1100 °C*

The microstructures of the test bars crept at 1100 °C had an appearance similar to the ones crept at 1000 °C to 9.9% strain. Many of the WC grain boundaries contained a film of the Co-rich binder phase, see Figs. 15 and 16. A number of the WC grain surfaces facing these grain boundary films had a saw-tooth like appearance (Figs. 15 and 16). The angles between the step facets on these grain surfaces were measured to 120° and 90° in Figs. 15b and 16c, respectively. Cr carbides were also observed in the Cr-doped material at this temperature.

The intergranular cavitation in the microstructures of the test bars crept at 1100 °C was, however, not as pronounced as after creep deformation at 1000 °C. The limited number of intergranular cavities that formed (Figs. 15 and 16) was reflected in a smaller increase in the intergranular volume fractions, see Table 4. Mean intergranular volume fractions of (11.2 ± 0.3) % and (11.6 ± 0.3) % were determined in the

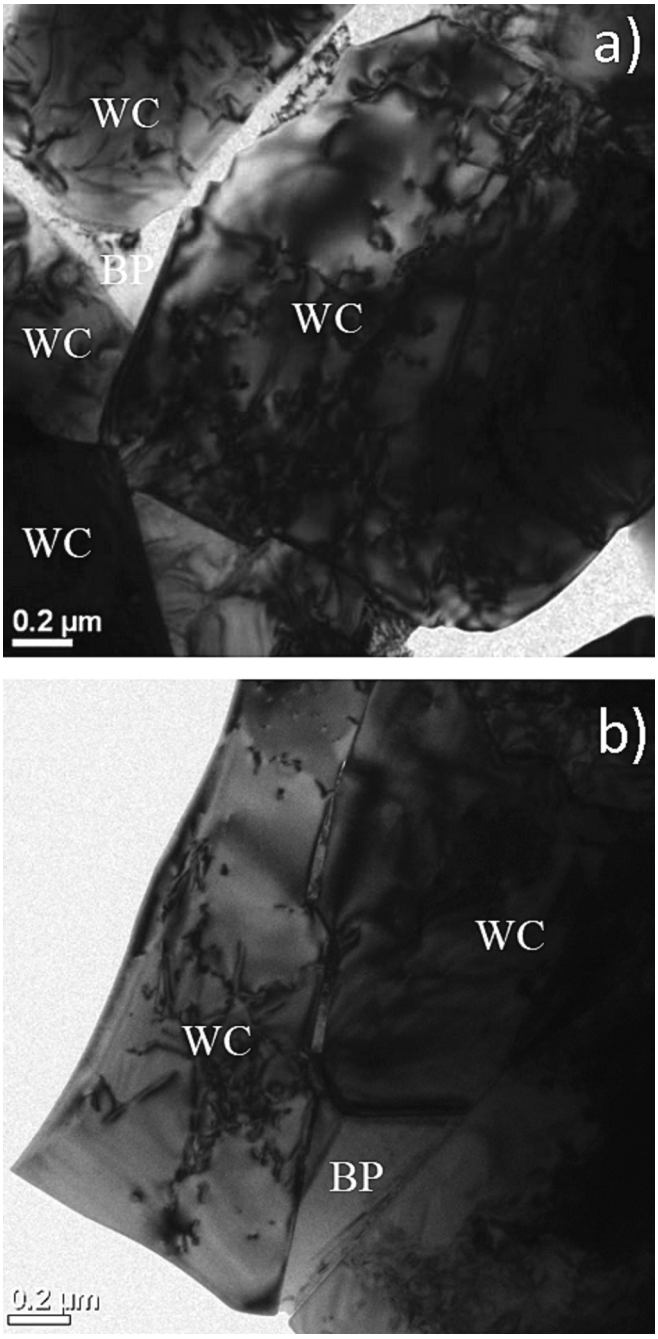

Fig. 11. TEM micrograph of the (a) un-doped material creep tested at 1000 °C to 10% strain and (b) the Cr-doped material creep tested at 1000 °C to 10% strain.

un-doped (8.7% strain) and Cr-doped (7.5% strain) materials, respectively.

The mean WC linear intercept length perpendicular to the axis of the test bar was considerably longer than in the as-sintered test bars also after creep deformation at 1100 °C, see Table 3. The values were (1.51 ± 0.06) μm for the un-doped material, and (1.50 ± 0.06) μm for the Cr-doped material. The mean WC linear intercept lengths determined parallel to the axis of the test bars were, on the other hand, virtually unchanged as compared to the as-sintered conditions, see Table 3. This value was (1.38 ± 0.08) μm for both the un-doped and Cr-doped test bar.

The sections taken parallel and perpendicular to the load axis showed a pronounced variation in the number density of binder phase film containing WC grain boundaries with distance from the centre of the test bar, see Table 5. There was a clear increase in the number density when going from the centre of the test bar to the rim of the cross-section, i. e. below the surface of the gauge length (Table 5). The un-doped test bar showed a slightly higher average number density of film containing grain boundaries on the section taken perpendicular to the load axis. An average number density of $(20.5 \pm 8.4) \times 10^{-3}$ μm^{-2} and $(18.8 \pm 6.3) \times 10^{-3}$ μm^{-2} was determined on the perpendicular and parallel sections, respectively, see Table 5. The microstructure of the crept Cr-doped test bar had a higher number density of film containing grain boundaries, and there was a clear difference between the number densities determined on the sections taken perpendicular and parallel to the load axis. An average number density of $(47.9 \pm 6.9) \times 10^{-3}$ μm^{-2} and $(28.0 \pm 3.3) \times 10^{-3}$ μm^{-2} was determined on the perpendicular and parallel sections, respectively, see Table 5.

3.4. Thermodynamic calculations

The equilibrium volume fraction of binder phase at 1000 and 1100 °C of both un-doped and Cr-doped materials was calculated, as well as the volume fraction of chromium carbide M_7C_3 (M = Cr, Co, W) in the Cr-doped material, see Table 6. The chromium addition gives a higher binder volume fraction, especially at 1100 °C, but the amount of chromium carbide is low. The calculated liquidus temperature is considerably lower for the Cr-doped material, 1261 °C compared to 1319 °C for the un-doped material.

4. Discussion

It has previously been established that WC-Co microstructures become stable as diffusion in the binder phase ceases between 900 and 800 °C when they are slowly cooled from high sintering or heat treatment temperatures [35]. The very fast cooling from the creep test temperatures down to around 800 °C in the present study ensures that the investigated microstructures of the crept test bars are representative of the microstructures that evolved during creep testing.

Comparing the average strain rate obtained at 1100 °C (4.8×10^{-5} and 4.2×10^{-5} s^{-1} for un-doped and Cr-doped materials, respectively) with the strain rates at 1000 °C (11×10^{-5} and 4.1×10^{-5} s^{-1}) shows that the selection of 300 MPa stress at 1100 °C gave a good match to the strain rates at 900 MPa and 1000 °C. It also shows that the effect of Cr to reduce the strain rate was much larger at 1000 °C than at 1100 °C.

4.1. WC grains

The mean linear intercept lengths determined perpendicular and parallel to the load axis imply that the WC grains grew preferentially in the plane perpendicular to the load axis during compressive creep deformation, see Table 3. WC grain growth at 1000 °C was unexpected, since growth of WC grains usually requires a much higher temperature. Grain growth of WC is known to be limited by the interface reaction rather than by diffusion, and the slow interface reaction is believed to be caused by a slow nucleation of successive atomic layers onto WC surfaces [36]. However, WC grain growth during compressive testing of WC-13% Co at high temperatures (1100–1250 °C) was observed already by Lee et al. [21], but they saw no difference in WC grain size when measured in cross-sections made parallel and perpendicular to the load axis after deformation at 1200 °C. Also, annealing at 1200 °C did not produce any measurable grain growth.

Our observed preferential growth is in accordance with previous work on a fine grained WC-Co cemented carbide material creep tested in compression at 1000 and 1100 °C [15]. It was suggested that some dislocation glide in WC grains had formed dislocations emerging at the grain surface, there acting as nucleation sites for grain growth [15]. In the present work, the un-doped material crept at 1000 °C to a strain of 9.9% had a mean linear intercept length of (1.58 ± 0.06) μm perpendicular to the load axis. The time spent to reach this deformation was

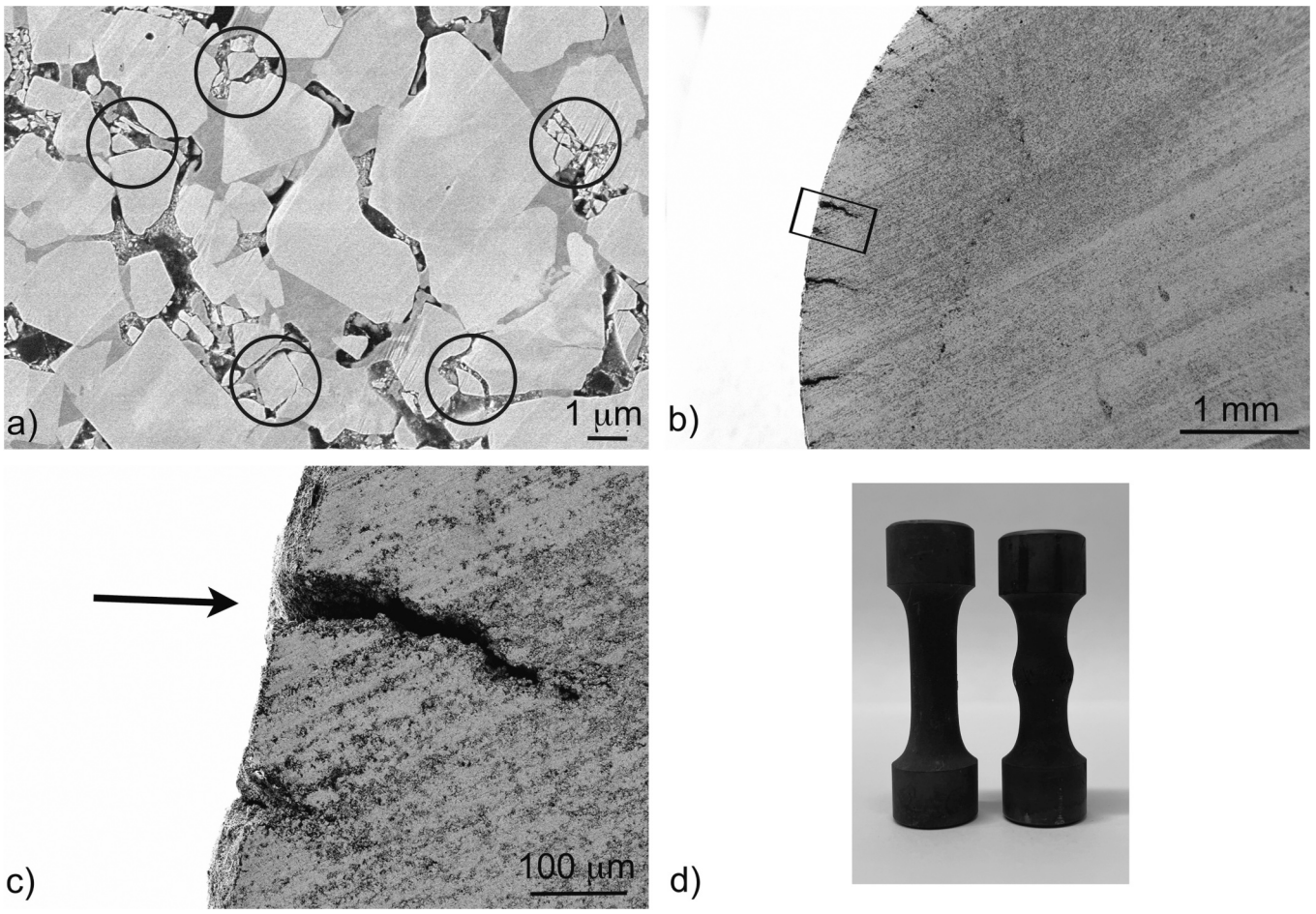

Fig. 12. Crack formation in the un-doped test bar crept at 1000 °C to 19.9% strain. A large number of the WC grains are cracked, encircled in (a), and the cross-section through the test bar shows radial cracks below the surface of the gauge length, framed in (b) and arrowed in (c). (c) is a higher magnification detail of the area marked in (b). (d) shows the undoped test specimen before and after creep testing performed at 1000 °C to 19.9% strain.

923 s. Creep deformation of the un-doped material at the higher temperature 1100 °C to a lower strain of 8.7% took 1800 s, and resulted in a mean linear intercept length of (1.51 ± 0.06) μm perpendicular to the load axis. A higher temperature and a longer time did, hence, not promote the growth of the WC grains in directions perpendicular to the compressive load axis. A larger strain was, on the other hand, associated with a larger mean linear intercept length perpendicular to the load axis. These observations agree with the proposition that WC grain growth is promoted by plastic deformation of WC grains [15]. Dislocations with a screw component emerging on a WC grain surface would create a spiral defect that may serve as a nucleation site for successive atomic layers of tungsten and carbon [15]. It may be expected that a higher strain would be associated with an increased defect density, and thereby an increased number of nucleation sites. This would in turn lead to an increased grain growth. In fact, a dependence of WC grain growth during sintering on WC dislocation density (more strictly WC crystal defect density) has recently been found [37].

An estimate of diffusion distances at the creep test temperatures implies that the transport of W and C in the Co-rich binder phase would be sufficient for WC grain growth [38]. During 923 s at 1000 °C, the W atoms would be able to travel a distance of 0.7 μm, i. e. half of the average WC grain size in the as-sintered material. During 1800 s at 1100 °C this distance would be 2.2 μm, i. e. 1.6 times the average WC grain size after sintering. The transport of the interstitial C atoms in the Co-rich binder phase would be even faster [39].

WC grains are, as mentioned in the introduction, expected to deform plastically through dislocation motion at elevated temperatures [3]. A WC grain size increase perpendicular to the load axis caused by plastic deformation would require a WC grain size decrease parallel to the load axis. This was not observed; the mean linear intercept length of the WC grains along the load axis was virtually unchanged after creep testing. This suggests that there was only a limited plastic deformation of the WC grains under the applied compressive load. This is in accordance with the limited number of dislocations observed with TEM after creep testing (Fig. 11).

4.2. Intergranular microstructure

The number density of WC grain boundaries containing a film of the Co-rich binder phase clearly increased during creep deformation (Figs. 9, 10, 15, 16 and Table 5). After 9.9% strain at 1000 °C the increase was a factor of 5–6, and the same increase was found after 7.5% strain at 1100 °C in the Cr-doped material. This is similar to the increased number density found by Toller et al. studying WC grain boundaries after turning test [1]. This implies an infiltration of WC grain boundaries by the Co-rich binder phase during creep deformation. This phenomenon has also been observed in creep experiments on a fine grained WC-Co material, and it was suggested that the infiltration was a result of grain boundary sliding [15]. An applied compressive load will introduce a shear stress in WC grain boundaries, and thereby push adjacent WC grains apart, see Fig. 17. This separation may be accommodated by the infiltration of the Co-rich binder into the grain boundary. A higher number density of infiltrated grain boundaries was observed in the plane perpendicular to the load axis than in the plane

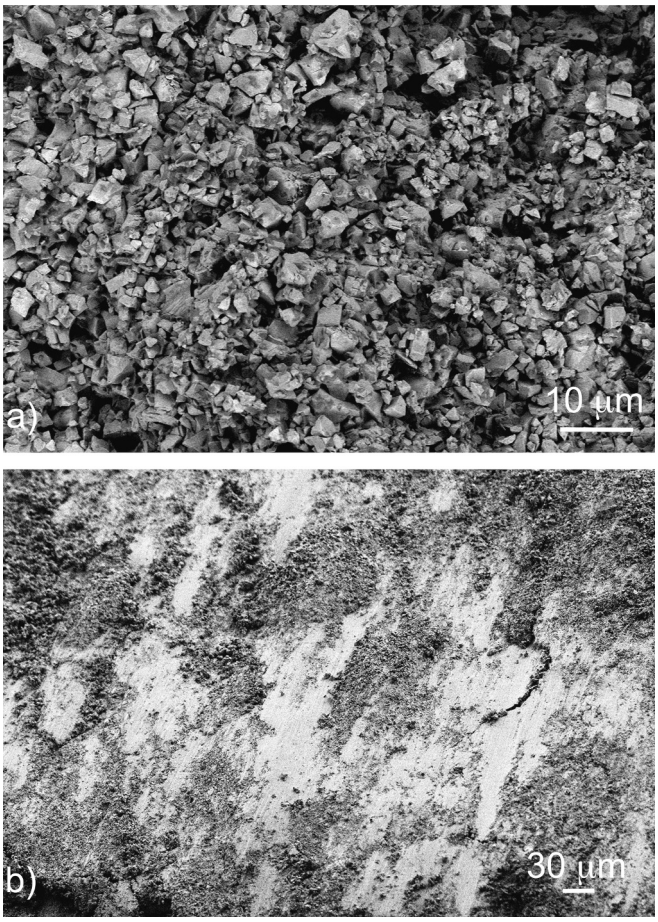

Fig. 13. The fracture surface of the Cr-doped test bar crept at 1000 °C to 17.1% strain. (a) Below the surface of the gauge length. (b) Close to the centre of the test bar.

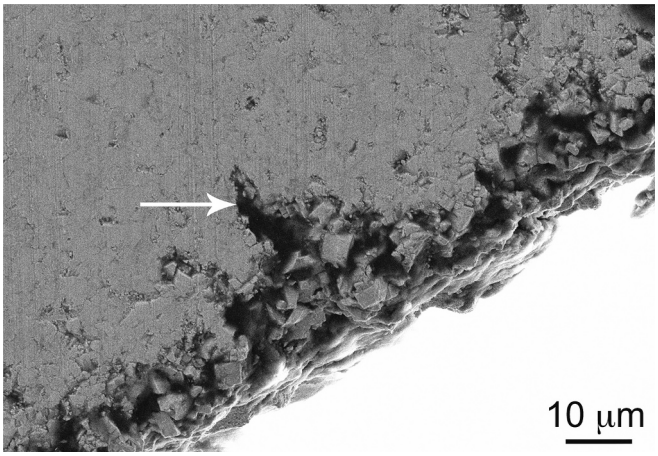

Fig. 14. A cross-section through the gauge length of the Cr-doped test bar crept at 1000 °C to 9.9% strain showing radial crack initiation (arrowed) at the surface of the gauge length.

parallel to the axis (Table 5). This would be consistent with the application of a compressive load on the test bar, see the schematics in Fig. 17. A section parallel to the load axis (Fig. 17a) would contain WC grain boundaries that were subjected to a shear stress during creep. These boundaries would not be expected to contain any larger amounts of infiltrated binder phase. A section perpendicular to the applied load

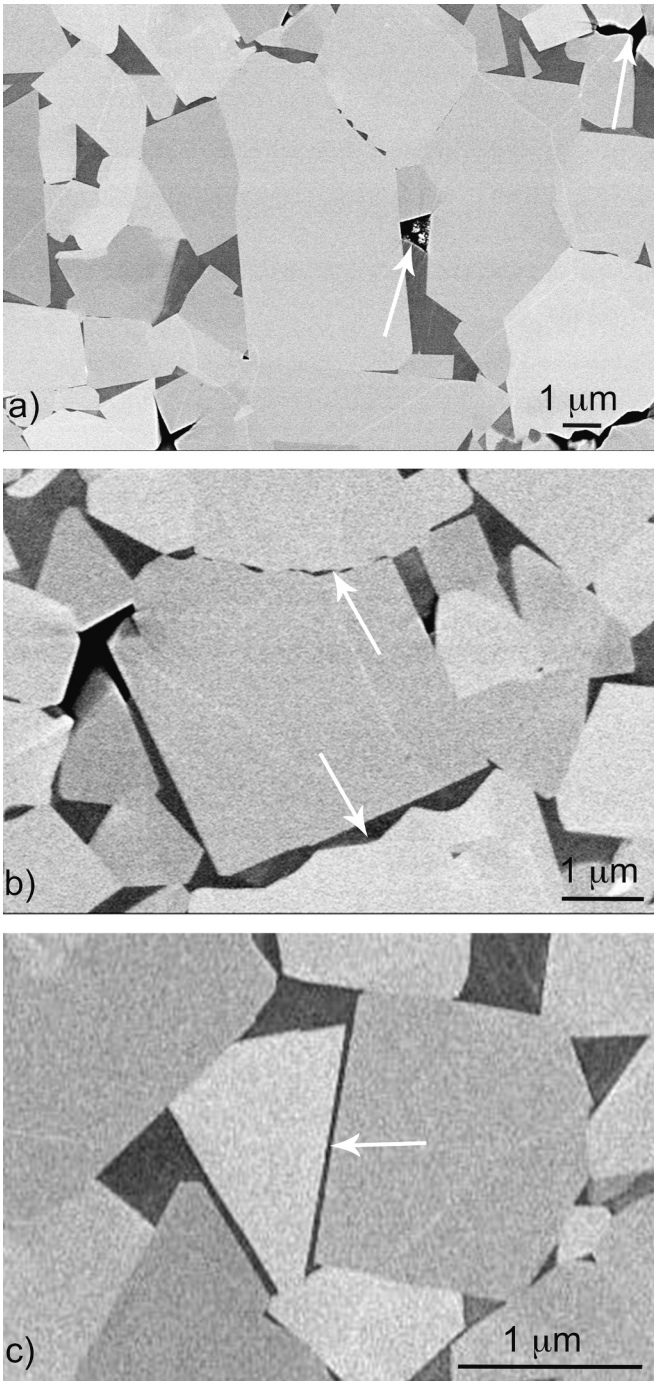

Fig. 15. (a) The general microstructure of the un-doped test bar crept at 1100 °C to 8.7% strain. The WC grains appear with bright contrast, the binder phase with dark, and the cavities (arrowed) with black contrast. (b) and (c) Higher magnification details showing Co-rich films at WC grain boundaries. Some WC grain surfaces, arrowed in (b), have a saw-tooth like appearance. Other WC grain boundaries contain a thin binder phase lamella, arrowed in (c). The WC grain surface arrowed in (b) has steps forming an angle of 120°.

(Fig. 17b) would, on the other hand, mainly contain WC grain boundaries that were subjected to a local tensile stress. As a consequence, a number of these boundaries would be infiltrated by the Co-rich binder phase, provided that the mobility of Co is sufficient under the creep test conditions. The number density of infiltrated WC grain boundaries was lower in the undoped material after 8.7% strain at 1100 °C, a factor of only 2–3 higher than in the as-sintered material.

A similar orientation dependence of the occurrence of infiltrated WC

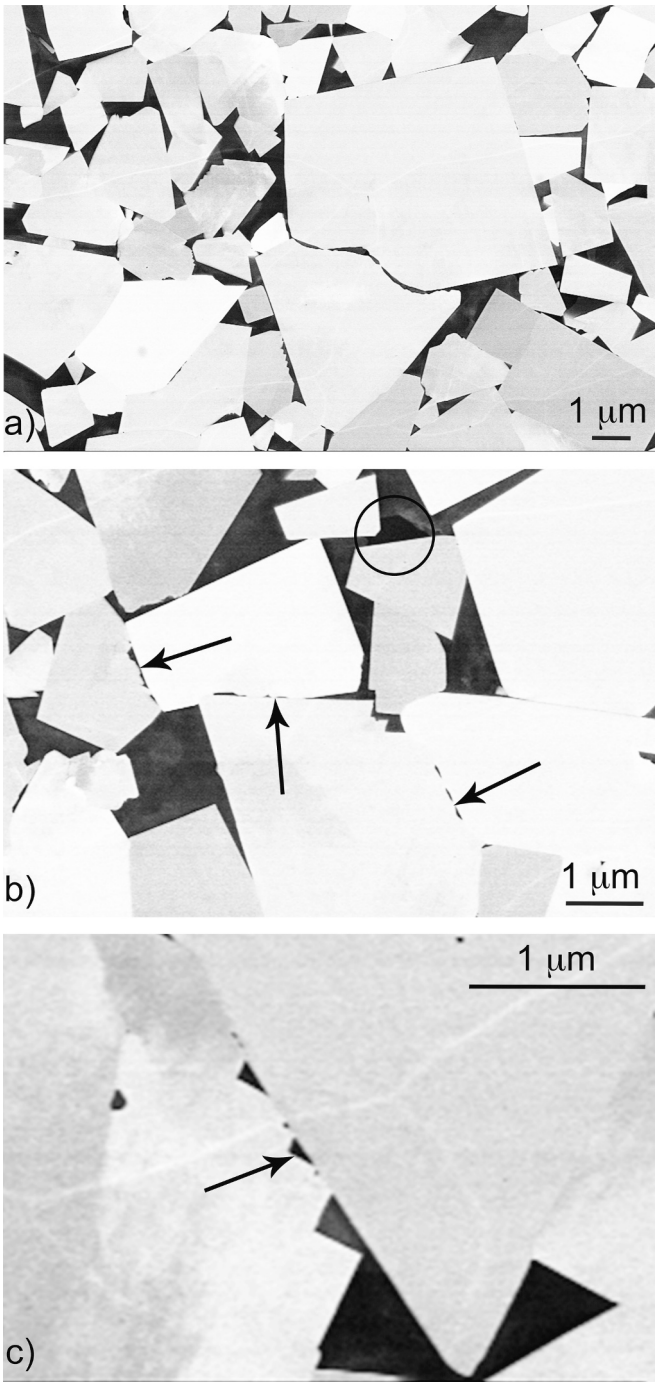

Fig. 16. (a) The general microstructure of the Cr-doped test bar crept at 1100 °C to 7.5% strain. The WC grains appear with bright and the binder phase with dark contrast. (b) and (c) Higher magnification details showing Co-rich films at WC grain boundaries. Some WC grain surfaces, arrowed in (b), have a saw-tooth like appearance. An example of a Cr carbide is encircled in (b). The WC grain surface arrowed in (c) has steps forming an angle of 90°.

Table 6
Calculated equilibrium volume fractions of binder phase and chromium carbide.

Material	Binder phase volume fraction [%]		M_7C_3 volume fraction [%]	
	1000 °C	1100 °C	1000 °C	1100 °C
Un-doped	10.85	11.18	–	–
Cr-doped	11.96	12.64	0.46	0.073

grain boundaries was found by Östby et al. [40]. They found that after a turning experiment the orientation of infiltrated boundaries was predominantly along the net compressive stress in the cutting insert (the third principal stress). They were also able to model the WC grain separation using microscale finite element modelling and found that the maximum WC separation occurred for such orientations [40].

At 1000 °C, the Co atoms would be able to travel distances of 0.5 and 0.9 μm during 923 and 2405 s, respectively, in the Co-rich binder phase [41]. These values correspond to only 0.4 and 0.6 times the average grain size in the as-sintered un-doped (923 s and 0.5 μm) and Cr-doped (2405 s and 0.9 μm) materials. It is therefore not surprising that Co diffusion is not sufficient to allow a full redistribution of the binder phase during creep deformation, and therefore a few vol% of cavities are formed (Table 4). During 1800 s at 1100 °C, the Co atoms would be able to travel a distance of 2 μm, i. e. 1.4 times the average WC grain size in the as-sintered materials. This seems sufficient to prevent most of the cavity formation (Table 4). The binder phase pockets on a section through the as-sintered microstructure (Fig. 4) are generally smaller than the WC grain sections. This implies that the mobility of Co under the applied creep conditions would be sufficient for infiltration of WC grain boundaries. An increased number density of infiltrated grain boundaries was observed at the rim of the cross-section, i. e. just below the surface of the gauge length (Table 5). This would be consistent with the need for an increased plane strain with increased distance from the centre of the test bar during a compressive creep test. It should be noted that relocation of the binder phase could occur not only due to diffusion but also through dislocation activity. On the other hand, Fig. 10 show only little presence of dislocations in the binder phase. Another argument for why diffusion of the binder phase is believed to be the primary contribution for the relocation is the decreased grain size of the binder phase [15].

The WC grain boundaries infiltrated by the Co-rich binder phase in the crept microstructures had two different morphologies. Some WC grains had a straight and well-defined interface towards the infiltrated Co (e. g. Fig. 14c), other WC grains had a saw-tooth like surface towards the grain boundary Co (e. g. Fig. 14b). An angle of 120° between the step facets on a WC grain surface (Fig. 14 b) would correspond to the angle between two adjacent prismatic plane surfaces on a freely growing WC grain [42]. The angle of 90° (Fig. 15c) would, under such growth conditions, correspond to the angle between the basal plane and a prismatic plane [42,43]. The development of these stepped WC grain surfaces suggests that a dissolution/reprecipitation process took place in the Co-rich binder phase that had infiltrated the original WC grain boundaries. This process would also be associated with WC grain growth.

Intragranular cavities were observed in all crept microstructures (Figs. 9, 10, 15). This would explain the increased intergranular volume fraction of the crept materials (Table 4), the effect being much larger at 1000 °C (around 3 vol% units increase in intergranular volume) than at 1100 °C (1.1 and 1.7 vol% units increase). It must be noted, though, that the volume fraction of binder might increase at high temperatures. Thermodynamic modelling gave equilibrium binder phase contents of 10.9 and 12.0 vol% (un-doped and Cr-doped, respectively) at 1000 °C and 11.2 and 12.6 vol% at 1100 °C (Table 6). For both materials, the as-sintered volume fraction is estimated to 10.0 vol%, as also measured. It should be noted that the Cr addition gives a higher volume fraction of binder phase, especially at 1100 °C. Even if time is not sufficient to establish full thermodynamic equilibrium during creep testing, the volume fraction of binder might well be higher than in the as-sintered material, especially at 1100 °C. Clearly, since the binder volume fraction increased with a maximum of 0.9 and 2.0% units at 1000 °C, a large part of the increase in intergranular volume measured at 1000 °C (2.8 and 3.2% units) must be due to cavities. The much lower increase in intergranular volume at 1100 °C (1.1 and 1.7% units) could well to a large extent be due to an increased binder volume fraction, since the calculated maximum increase is 1.2 and 2.6% units.

The cavity formation suggests that unaccommodated grain boundary

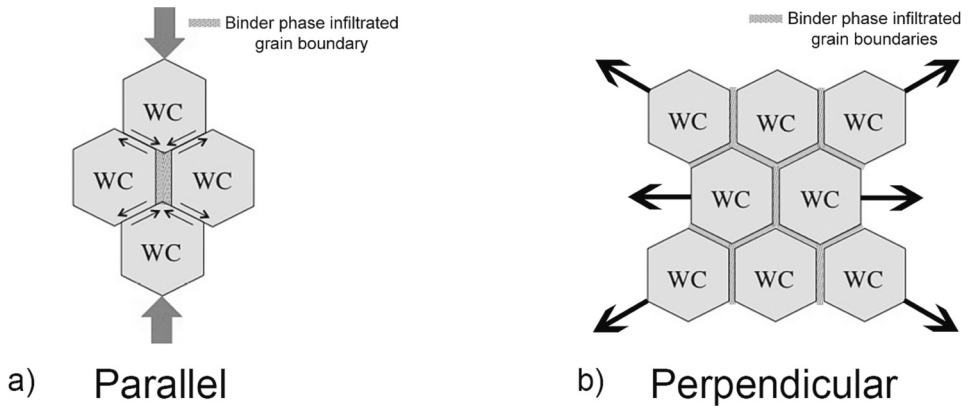

Fig. 17. Schematics illustrating grain boundary sliding and the infiltration of WC/WC grain boundaries by the Co-rich binder phase in a section parallel to (a) and perpendicular to (b) the compressive load axis.

sliding also took place during creep deformation. The infiltration of Co into the WC grain boundaries would not only require a sufficiently high Co mobility, but also a neighbouring supply of Co. The observed redistribution of the binder phase may, locally, result in binder deficient areas that would impede the diffusion of Co into WC grain boundaries that experience a local tensile stress during grain boundary sliding. As a result, intragranular cavities would form, although the formation of free surfaces is an energy costly process [42]. Calculated WC surface energies are in the range 3.37–9.02 Jm^{-2}, depending on the crystallographic orientation of the surface and its termination (W or C) [41]. The energy of a free Co surface has been calculated to be in the range 2.03–2.53 J m^{-2}, depending on its crystallography [44]. The formation of cavities during plastic deformation of WC-Co is in agreement with earlier observations [1,15,45].

4.3. Deformation mechanisms

From the observed microstructure for both materials crept at both 1000 and 1100 °C, evidence for grain boundary sliding was found. This is as expected for these temperatures and the high loads that was used [18].

At 1000 °C the Cr-doped material showed a much higher creep resistance than the un-doped material. In both materials the same deformation mechanisms, accommodated and unaccommodated grain boundary sliding, appeared to operate. The deformation occurred, however, on different time scales, suggesting that an additional creep mechanism was active, and that this mechanism was rate limiting in the deformation process.

One obvious candidate is the very large WC grain growth that took place perpendicular, but not parallel, to the compressive axis. During the 9.9% compression of the Cr-doped material at 1000 °C, WC grains grew from 1.40 to 1.59 μm, i.e., 13.6%, perpendicular to the load axis but remained in size parallel to the axis. Since the grain size perpendicular to the load axis was measured in cross-sections both perpendicular and parallel to the load axis with the same result, the grains must have grown in all directions perpendicular to the load axis, i.e., both radial and tangential. This means that each grain increased 29.0% in area in this plane but remained at the same size parallel to the axis. Therefore, the volume of each grain increased by 29.0%, and thus the number density of grains decreased to 77.5% of the original number density. Obviously, a number of small grains have been dissolved, and W and C have diffused though the binder and re-precipitated on the available faces of larger grains, which of course were the faces not in direct compressive contact with other WC grains but those in contact with binder phase, oriented more or less along the load axis.

If all dissolution of small WC grains could contribute to the total compressive strain, the directional coarsening would correspond to a compressive strain of 22.5%. However, this cannot occur only by diffusion itself since the WC grain boundaries under compressive stress are not infiltrated with binder phase and thus are not accessible to dissolution in the binder. Instead, a major effect of W and C diffusion in the binder must be the selective dissolution of WC thus facilitating grain boundary sliding. Thus, directional coarsening must also act as an accommodation mechanism for grain boundary sliding.

Another accommodation mechanism is of course binder phase lamella formation; the average number density of infiltrated grain boundaries, 40×10^{-3} μm^{-2}, represents only some 4% of all boundaries, and with a lamella width of perhaps 100 nm each lamella represents a strain perpendicular to the load axis of 6%. This results in a perpendicular expansion of only 0.25%, and with a constant volume fraction of binder phase corresponds to a contribution to the compressive strain of only 0.5%. However, this redistribution serves as an important accommodation mechanism for grain boundary sliding. It also gives access for directional grain growth, i.e., dissolution and reprecipitation, to operate.

The formation of cavities shows that the binder phase doesn't have the time to redistribute. This is in contrast to what has been reported for materials tested at 1200 °C at low strain rates where the binder phase has migrated to the edges of the test material [46].

The formation of up to 3 vol% cavities is not expected to give any direct effect on the compressive strain. But in addition to directional grain growth and grain boundary infiltration, cavity formation of course also serves as an accommodation mechanism for grain boundary sliding. The local compressive strain in the volume where the microstructure was studied may be calculated from the maximum diameter of the creep tested specimens. After 9.9% compression at 1000 °C this diameter had increased from 6.30 to 7.24 mm or 15%, corresponding to a 32% area expansion. This corresponds to a compressive strain of 22% (accounting also for the 3 vol% cavity formation). This value can then be compared with the calculated maximum compressive strain due to redistribution of WC and binder from grain coarsening and binder lamella formation found above, 22.5% and 0.5%, respectively. The fact that the total compressive strain is the same as the strain that corresponds to redistribution of WC and binder again shows that grain boundary sliding is an integral part of the deformation. Clearly grain boundary sliding must be operating in addition to redistribution. This is in good agreement with the findings of Buss, who found that the creep deformation rate at high temperature of the WC skeleton without binder phase is much lower (virtually absent) than in WC-Co, where the presence of binder phase enables grain boundary sliding and thus plastic deformation, thereby avoiding brittle fracture [7].

So, the total 22% compressive strain can be explained both by redistribution of binder phase and WC by diffusion (and perhaps some little dislocation activity), enabling grain boundary sliding. Also, cavity

formation contributes to grain boundary sliding. The fact that only 9.9% compressive strain was recorded is of course due to the shape of the specimen. Most of the strain is localised to the middle part of the gauge length where the specimen bulges out, and here the strain is much larger than the mean strain.

Thus, we have two dominating mechanisms, grain growth (strictly grain coarsening) and grain boundary sliding, and the former is rate controlling since it is an accommodation mechanism for grain boundary sliding.

4.4. Effect of chromium: 1000 °C

The creep tests at 1000 °C carried out to 9.9% strain took 923 s for the un-doped test bar, and 2405 s for the Cr-doped test bar; i.e., a factor of 2.6 longer time was required in order for the Cr-doped test bar to reach this strain. One effect of the Cr addition is the formation of a low volume fraction of chromium carbide M_7C_3 that remains after creep testing. According to the thermodynamic calculations, the equilibrium volume fraction of chromium carbide is only 0.5 vol% at 1000 °C (and even smaller, 0.07 vol% at 1100 °C), see Table 6. As the size of chromium carbide grains is small and they usually replace part of a binder phase volume (Figs. 4b, 8a and 15b), it is not likely that they can decrease the creep deformation rate much. However, the fact that the WC grain size increases perpendicular to the compressive load axis after the creep tests at 1000 °C was similar in the two test bars, see Table 3, means that the WC grain growth rate was lower in the Cr-doped material.

The results in the present investigation thus imply that the obtained strain during creep deformation was associated with WC grain growth perpendicular to the compressive load axis. The addition of Cr to a WC-Co material is well known to be a WC grain growth inhibitor [22,23]. Atom probe tomography has shown that chromium segregates to WC/Co phase boundaries [47]. The equilibrium segregation of Cr in the binder phase was estimated to 0.4 monolayer in material heat treated at 1000 °C, and the energy of segregation was calculated to 0.22 eV/Cr atom (21 kJ/mol Cr) from the atom probe data. This Cr segregation may explain the WC grain growth inhibiting effect during sintering of Cr additions to WC-Co cemented carbide materials. It is reasonable to assume that the same mechanism lies behind the observed effect of Cr additions on the creep strength, since grain growth seems to be responsible for a large part of the compressive strain.

The idea is then that Cr atoms at the WC grain surfaces need to be replaced by W or C in order for a WC grain to grow in a Cr-doped binder phase environment. The replacement of Cr by W, and/or C, is a process that would require time and thereby slow down grain growth. This would be consistent with a slower WC grain growth in the Cr-doped material, which suggests that WC grain growth perpendicular to the compressive load axis would be rate limiting in the creep deformation process.

4.5. Effect of chromium: 1100 °C

The grain growth inhibiting effect of Cr is expected to work also at 1100 °C, since the equilibrium segregation of Cr at phase boundaries is only marginally smaller (0.32 monolayers compared to 0.36 monolayers at 1000 °C). After all, Cr works well as a grain growth inhibitor at the much higher sintering temperatures (1400–1450 °C) [23]. However, the effect was weak; the time to 7.5% strain was only 20% longer compared to the un-doped material (1800 s compared to 1500 s). As a comparison, at 1000 °C the Cr-doped material took 160% longer time to deform 9.9% than the un-doped material. Surprisingly, the WC grain growth after 1800 s at 1100 °C was about the same in the two materials. One striking difference in the microstructure is that in the un-doped material the number of infiltrated WC grain boundaries was much lower than in the doped material (Table 5). It was also lower than in both materials after creep at 1000 °C, and one reason for this might be the lower stress, 300 MPa instead of 900 MPa, since WC grain boundary infiltration is believed to be driven by stress [7]. This much lower density of binder phase lamellae (around 20 compared to almost 50×10^{-3} μm^{-2}) means that more than twice as many grains in the Cr-doped material has contact with a binder phase lamella and can grow by W and C diffusion. The fact that the average growth is still about the same shows that the effect of Cr hindering the grain growth still is in operation.

The much lower binder phase lamella density in the un-doped material is probably connected to the lower intragranular volume, that might be due to the lower equilibrium binder phase volume in the un-doped material. The effect of Cr on equilibrium binder phase volume is rather large, 12.6 compared to 11.2 vol%, and the effect on the liquidus temperature is also considerable, 1261 °C compared to 1319 °C. The measured volume, maximum 11.7 vol% compared to 11.1 vol% in the un-doped material, is smaller than the equilibrium value, as expected, but obviously still large enough to give a large difference in binder lamella formation at the lower compressive stress of 300 MPa.

4.6. Practical applications

The effect on Cr addition on compressive creep strength is clearly interesting for applications where WC-Co is used under high compressive loads and high temperatures such as rock drilling. In fact, based on the present results new Cr-containing grades for rock drill buttons have been developed, and found to have a higher wear resistance that the corresponding Cr-free grade [48]. As an example, in a top hammer drilling test in a mine the Cr-containing button gave 286 drill meters per mm wear whereas the Cr-free button only gave 183 drill meters. Cr-containing rock drill bits are now commercially available [48].

5. Conclusions

WC-10 vol% Co cemented carbide with a WC grain size of 1.4 μm (linear intercept), both with and without 0.6 wt% addition of Cr, was exposed to creep testing at 1000 °C with 900 MPa compressive stress and at 1100 °C with 300 MPa compressive stress.

(1) At 1000 °C the creep rate of Cr-doped WC-Co was much smaller than that of the undoped material. Creep to approximately 9.9% strain took only 903 s in undoped but 2405 s in Cr-doped material.

(2) At 1100 °C the creep rate of Cr-doped material was also smaller than that of undoped material. Creep testing for 1800 s gave a strain of 8.7% for undoped material but only 7.5% for Cr-doped material.

(3) Preferential WC grain growth (strictly grain coarsening) takes place in the plane perpendicular to the load axis during compressive creep testing at 1000 and 1100 °C. No change in grain size occurred parallel to the load axis. This means that the grain volume increased and the number density of grains decreased. This grain coarsening corresponds to a maximum compressive strain of 22% after 9.9% strain at 1000 °C.

(4) Binder phase also redistributes by diffusion and possibly also dislocation movement, partly by infiltrating WC grain boundaries oriented more or less parallel to the load axis. This redistribution itself contributes very little to the compressive strain, only 0.5% after 9.9% strain at 1000 °C, but it increases grain growth by setting more WC grains in contact with binder phase.

(5) The high load used in these experiments led as expected to WC grain boundary sliding, accommodated by the coarsening of WC grains and redistribution and infiltration of the binder phase in WC grain boundaries, both at 1000 and 1100 °C.

(6) The formation of intergranular cavities during creep testing implies that also unaccommodated WC grain boundary sliding occurs, especially at 1000 °C.

(7) The total maximum compressive stress can be estimated from the expansion of the creep specimen perpendicular to the load axis. After 9.9% strain at 1000 °C the total strain was estimated to 22%. This is about the same strain as calculated from the redistribution of WC and

binder phase.

(8) Consequently, the dominating creep mechanism was grain boundary sliding accommodated by redistribution and directional growth of WC grains.

(9) WC grain growth was creep rate controlling for both materials investigated in this study. The Cr doping, previously found to segregate to WC/binder phase boundaries, slowed down WC grain growth and resulted in an improved creep resistance under compression.

(10) Cr addition leads to larger binder phase volume, more infiltrated WC grain boundaries and more growing WC grains. This effect counteracts the effect of Cr to inhibit grain growth and makes the effect of Cr addition much smaller at 1100 °C than at 1000 °C.

Declaration of Competing Interest

The authors declare the following financial interests/personal relationships which may be considered as potential competing interests:

Hans-Olof Andren reports financial support was provided by Swedish Research Council. Susanne Norgren, Anders Nordgren reports a relationship with Sandvik Coromant Sweden that includes: employment and equity or stocks. Susanne Norgren, Anders Nordgren has patent #EP 3274482 B1 issued to Sandvik Intellectual Property AB.

Data availability

All data used in the research are given in the article.

Acknowledgements

Sandvik Coromant AB, the Rock Tools Division of Sandvik Mining, and Seco Tools AB are thanked for fruitful discussions and financial support. Financial support was also received from the Swedish Research Council (VR).

References

[1] L. Toller-Nordström, J. Östby, S. Norgren, Towards understanding plastic deformation in hardmetal turning inserts with different binders, Int. J. Refract. Met. Hard Mater. 94 (2021) 105309.
[2] F. Ueda, H. Doi, F. Fujiwara, Bend deformation and fracture of WC-Co at elevated temperatures, Trans. Jpn. Inst. Met. 18 (1977) 247–256.
[3] S. Lay, J. Vicens, F. Osterstock, High temperature creep of WC-Co alloys, J. Mater. Sci. 22 (1987) 1310–1322.
[4] R. Schaller, D. Mari, M. Maamouri, J.J. Ammann, Mechanical behaviour of WC-11 wt.% Co studied by bending tests, internal friction and electron microscopy, J. Hard. Mater. 3 (1992) 351–362.
[5] D. Mari, U. Marti, P.C. Silva, A new photolithographic technique to detect the local deformation of materials: application to WC–Co composites, Mater. Sci. Eng. A158 (1992) 203–206.
[6] D. Mari, S. Bolognini, G. Feusier, T. Viatte, W. Benoit, Experimental strategy to study the mechanical behaviour of hardmetals for cutting tools, Int. J. Refract. Met. Hard Mater. 17 (1999) 209–225.
[7] G. Östberg, K. Buss, M. Christensen, S. Norgren, H.-O. Andrén, D. Mari, et al., Mechanisms of plastic deformation of WC–Co and Ti(C,N)–WC–Co, Int. J. Refract. Met. Hard Mater. 24 (2006) 135–144.
[8] F. Ueda, H. Doi, F. Fujiwara, Tensile creep of WC-10% Co and WC-10 % TaC-10 % Co at elevated temperatures, Trans. Jpn. Inst. Met. 16 (1975) 591–600.
[9] G. Wirmark, C. Chatfield, G.L. Dunlop, Tensile creep of WC-Co cemented carbides at 800-900 °C, in: 2nd International Conference on the Science of Hard Materials, Adam Hilger Ltd, Accord, MA (USA), 1986, pp. 669–678.
[10] B. Roebuck, S. Moseley, Tensile and compressive asymmetry in creep and monotonic deformation of WC/Co hardmetals at high temperature, Int. J. Refract. Met. Hard Mater. 48 (2015) 126–133.
[11] K. Mingard, S. Moseley, S. Norgren, H. Zakaria, D. Jones, B. Roebuck, Microstructural observations of high temperature creep processes in hardmetals, Powder Metall. 64 (2) (2021) 97–107.
[12] K. Maier, T. Klünsner, M. Krobath, P. Pichler, S. Marsoner, W. Ecker, et al., Creep behaviour of WC-12 wt% Co hardmetals with different WC grain sizes tested in uniaxial tensile and compression step-loading tests at 700 °C and 800 °C, Int. J. Refract. Met. Hard Mater. 100 (2021) 105633.
[13] J.T. Smith, J.D. Wood, Elevated temperature compressive creep behaviour of tungsten carbide-cobalt alloys, Acta Metall. 16 (1968) 1219–1226.
[14] T. Sakuma, High-temperature plastic flow in cemented carbides and cermets, Key Eng. Mater. 108-10 (1995) 435–448.
[15] M.A. Yousfi, J. Weidow, A. Nordgren, L.K.L. Falk, H.-O. Andrén, Deformation mechanisms in a WC-Co based cemented carbide during creep, Int. J. Refract. Met. Hard Mater. 49 (2015) 81–87.
[16] R. Useldinger, U. Schleinkofer, Creep behaviour of cemented carbides - influence of binder content, binder composition and WC grain size, Int. J. Refract. Met. Hard Mater. 62 (2017) 170–175.
[17] G. Östberg, H.-O. Andrén, Microstructural changes during wear by plastic deformation of cemented carbide and cermet cutting inserts, Metall. Mater. Trans. A 37 (2006) 1495–1506.
[18] K. Buss, High temperature deformation mechanisms of cemented carbides and cermets, PhD thesis, Ecole Polytechnique Fédérale de Lausanne, 2004.
[19] M.V.G. Petisme, M.A. Gren, G. Wahnström, Molecular dynamics simulation of WC/WC grain boundary sliding resistance in WC–Co cemented carbides at high temperature, Int. J. Refract. Met. Hard Mater. 49 (2015) 75–80.
[20] J. Weidow, H.-O. Andrén, Binder phase grain size in WC–Co-based cemented carbides, Scr. Mater. 63 (2010) 1165–1168.
[21] I.C. Lee, H. Hondo, T. Sakuma, Nonuniform carbide grain growth during high-temperature compressive deformation in WC–13 wt.% Co, Scr. Metall. Mater. 28 (1993) 97–102.
[22] K. Hayashi, Y. Fuke, H. Suzuki, Effects of addition carbides on the grain size of WC-Co alloy, J. Jpn. Soc. Powder Metall. 19 (1972) 67–71.
[23] J. Weidow, S. Norgren, H.-O. Andrén, Effect of V, Cr and Mn additions on the microstructure of WC–Co, Int. J. Refract. Met. Hard Mater. 27 (2009) 817–822.
[24] K. Brookes, World Directory and Handbook of Hardmetals and Hard Materials, 6th ed, International Carbide Data, 1996.
[25] R. M'Saoubi, S. Ruppi, Wear and thermal behaviour of CVD α-Al_2O_3 and MTCVD Ti(C,N) coatings during machining, CIRP Ann. Manuf. Technol. 58 (2009) 57–60.
[26] P.A. Dearnley, A.N. Grearson, Evaluation of principal wear mechanisms of cemented carbides and ceramics used for machining titanium alloy IMI 318, Mater. Sci. Technol. 2 (1) (1986) 47–58.
[27] P.D. Hartung, B.M. Kramer, B.F. von Turkovich, Tool wear in titanium machining, CIRP Ann. Manuf. Technol. 31 (1) (1982) 75–80.
[28] T. Kitagawa, A. Kubo, K. Maekawa, Temperature and wear of cutting tools in high-speed machining of Inconel 718 and Ti-6Al-6V-2Sn, Wear 202 (1997) 142–148.
[29] J.-S. Zhang, High Temperature Deformation and Fracture of Materials, Woodhead Publishing Limited, 2010.
[30] ASTM, Guide for Metallographic Identification of Microstructure in Cemented Carbides B657–11, 2012, pp. 1–5.
[31] International Organization for Standardization, ISO 4499-2:2008. Hardmetals - Metallographic Determination of Microstructure. Part 2: Measurement of WC Grain Size, International Standards Organization, 2008, pp. 1–17.
[32] ASTM, Standard Test Methods for Determining Average Grain Size E112–10, 2012, pp. 1–27.
[33] K. Mannesson, I. Borgh, A. Borgenstam, J. Ågren, Abnormal grain growth in cemented carbides - experiments and simulations, Int. J. Refract. Met. Hard Mater. 29 (2011) 488–494.
[34] S. Lay, HRTEM investigation of dislocation interactions in WC, Int. J. Refract. Met. Hard Mater. 41 (2013) 416–421.
[35] M. Hellsing, High resolution microanalysis of binder phase in as sintered WC–Co cemented carbides, Mater. Sci. Technol. 4 (1988) 824–829.
[36] K. Mannesson, J. Jeppsson, A. Borgenstam, J. Ågren, Carbide grain growth in cemented carbides, Acta Mater. 59 (2011) 1912–1923.
[37] J. Weidow, E. Ekström, M. Kritikos, S. Norgren, Impact of crystal defects on the grain growth of cemented carbides, Int. J. Refract. Met. Hard Mater. 72 (2018) 199–202.
[38] A. Davin, V. Leroy, D. Coutsouradis, L. Habraken, Comparison of the diffusion of some substitution elements in nickel and cobalt, Cobalt 19 (1963) 51–56.
[39] T. Hehenkamp, Diffusion und Elektrotransport von Kohlenstoff in Kobalt, Acta Metall. 14 (1966) 887–893.
[40] J. Östby, L. Toller-Nordström, S. Norgren, Insights into plastic deformation and binder lamella orientation in hardmetal turning inserts, Int. J. Refract. Met. Hard Mater. 103 (2022) 105779.
[41] R.C. Ruder, C.E. Birchenall, Cobalt self-diffusion: a study of the method of decrease in surface activity, J. Met. 3 (1951) 142–146.
[42] Villars P (chief editor). WC crystal structure, PAULING FILE. In: Inorganic Solid Phases. SpringerMaterials (online database). Springer, Heidelberg, https://materials.springer.com/isp/crystallographic/docs/sd_1715927 (accessed March 7, 2023).
[43] T. Yamamoto, Y. Ikuhara, T. Sakuma, High resolution transmission electron microscopy study in VC-doped WC–Co compound, Sci. Technol. Adv. Mater. 1 (2000) 97–104.
[44] M.V.G. Petisme, S.A.E. Johansson, G. Wahnström, A computational study of interfaces in WC–Co cemented carbides, Model. Simul. Mater. Sci. Eng. 23 (2015) 45001.
[45] H. Schmid, D. Mari, W. Benoit, C. Bonjour, The mechanical behaviour of cemented carbides at high temperatures, Mater. Sci. Eng. A 105 (1988) 343–351.
[46] S. Humphry-Baker, L. Vandeperre, Creep deformation of WC hardmetals with Fe-based binders, Int. J. Refract. Met. Hard Mater. 95 (2021) 105462.
[47] M.A. Yousfi, S. Norgren, H.-O. Andrén, L.K.L. Falk, Chromium segregation at phase boundaries in Cr-doped WC-Co cemented carbides, Mater. Char 144 (2018) 48–56.
[48] A. Nordgren, A. Ekmarker, S. Norgren, A rock drill button, in: Patent EP 3 274 482 B1 (2016), US 10,895,001 B2, 2021.